Landsat 9 Thermal Infrared Sensor 2 (TIRS-2) Stray Light Mitigation and Assessment

Matthew Montanaro, Joel McCorkel, June Tveekrem, John Stauder, Eric Mentzell, Allen Lunsford, Jason Hair, and Dennis Reuter

***Abstract*— The Thermal Infrared Sensor 2 (TIRS-2) payload for the Landsat 9 mission closely follows the design of the TIRS instrument currently flying aboard Landsat 8. The TIRS-2 instrument, however, incorporates an important design change to mitigate the stray light issue that plagued the TIRS instrument. Shortly after the launch of Landsat 8 in 2013, calibration errors due to stray light artifacts were observed in Earth imagery from TIRS with magnitudes of 4% (10.8 μm band) and 8% (12.0 μm band). Out-of-field scans of the Moon were conducted to map the angles from which off-axis radiance was detected on the focal plane arrays. Optical modeling, constrained by reverse ray traces of the lunar data, identified the primary scattering sources within the TIRS telescope, and these results informed the locations and design of mitigating baffles for TIRS-2. The effect of the modifications to the TIRS-2 instrument was tested preflight through thermal vacuum (TVAC) characterization tests, and the optical models were updated to be consistent with the measured data. Preliminary assessments indicated at least an order of magnitude reduction of the total signal due to scattering in TIRS-2. On-orbit lunar scans provided the final confirmations and demonstrated that the new design changes to TIRS-2 have reduced the primary out-of-field scattering by over 40x from the original TIRS design bringing the total scattering to 1% or less. More importantly, Earth imagery produced by Landsat 9 TIRS-2 does not show any stray-light-related artifacts, as was prevalent in the Landsat 8 TIRS imagery.**

***Index Terms*— Landsat, lunar scans, optical model, scattering, stray light, thermal infrared.**

I. Introduction

THE Thermal Infrared Sensor 2 (TIRS-2) is one of two instruments on-board the Landsat 9 (L9) observatory and was tasked with continuing the Landsat program's long-wave infrared imaging capabilities [1]. The TIRS-2 instrument shares a common design with the Landsat 8 (L8) TIRS instrument but is not a build-to-print rebuild due to changes in requirements and improvement in absolute accuracy. The TIRS design was modified to mitigate the stray light problem and to add redundancy for higher reliability allowing for longer mission life. The L8/TIRS instrument was found to have significant stray light, or scattering, within the optical system in which light from outside the field-of-view is recorded by the focal plane detectors. The additional signal on the detectors is scene-dependent and produced inconsistent and nonuniform banding artifacts in Earth imagery. Furthermore, the extra signal on the detectors caused radiometric calibration errors up to 8% [2]. The image artifacts and calibration errors were mostly corrected for in post-processing; however, the lessons learned from the L8/TIRS design were applied to the L9/TIRS-2 design to help avoid the issue.

When the TIRS-2 instrument for Landsat 9 was authorized, it was required to closely follow the design of TIRS. The instrument is a $\pm 7.5^\circ$ field-of-view (FOV) push-broom imager that covers the standard Landsat swath of 185 km from a 705 km orbit. A four-element refractive telescope images onto a focal plane consisting of three 512 by 640-pixel detector arrays staggered to provide the necessary swath width. Each detector array has two spectral filters placed over roughly 70 pixel rows to provide two spectral channels centered at 10.8 and 12.0 μm in wavelength with bandwidths of 0.8 and 1.0 μm, respectively. The rest of the array area is masked to provide dark pixels for trending purposes. Two rows of detectors in the two spectral regions are combined in the U.S. Geological Survey (USGS) Landsat image product generation system to produce calibrated image products known as Landsat 9 band 10 and band 11, for the 10.8 and 12.0 μm channels, respectively. The focal plane can also operate in a diagnostic mode in which multiple, selectable rows are read at a lower frame rate. In this "transmit-all" mode, TIRS-2 effectively operates as a framing imager (instead of in the push-broom mode).

The overall architecture of the TIRS-2 instrument remained the same as TIRS, but with the addition of electronic redundancies and optical design changes to correct for significant scattering in the optical system. The exact cause of the scattering in the TIRS design was well-known due to a major effort to measure the effect on-orbit on Landsat 8 and incorporate those measurements into a high-fidelity optical model [3]. The TIRS-2 telescope was slightly modified to drastically reduce the effect of the known scatter sources within the

Manuscript received March 1, 2022; revised April 25, 2022; accepted May 19, 2022. Date of publication May 23, 2022; date of current version June 9, 2022. This work was supported in part by the National Aeronautics and Space Administration (NASA) under Grant 80NSSC19K1441. *(Corresponding author: Matthew Montanaro.)*

Matthew Montanaro is with the Department of Hydrospheric and Biospheric Sciences, National Aeronautics and Space Administration (NASA) Goddard Space Flight Center (GSFC), Greenbelt, MD 20771 USA (e-mail: matthew.montanaro@nasa.gov).

Joel McCorkel is with the Department of Biospheric Sciences, NASA Goddard Space Flight Center, Greenbelt, MD 20771 USA.

June Tveekrem and Eric Mentzell are with the Department of Optics Branch, NASA Goddard Space Flight Center, Greenbelt, MD 20771 USA.

John Stauder is with the Space Dynamics Laboratory, Utah State University, Logan, UT 84322 USA.

Allen Lunsford and Dennis Reuter are with the Department of Planetary Systems, NASA Goddard Space Flight Center, Greenbelt, MD 20771 USA.

Jason Hair is with the Department of Flight Projects, NASA Goddard Space Flight Center, Greenbelt, MD 20771 USA.

Digital Object Identifier 10.1109/TGRS.2022.3177312

system. Preflight characterization tests were carefully planned to measure the effect of these modifications [4], [5]. Although a full out-of-field measurement was not possible due to limitations of the test setup, the high-quality test data combined with optical modeling indicated an order of magnitude reduction in scattering sources over the original TIRS instrument design. The limited measurements were incorporated into the optical model to predict the total effect of the residual stray light signals across the FOV. The measurements and the extrapolated model, while showing a significant reduction in scattering, still did not provide total assessment of the scattering magnitudes [5]. The final characterization of TIRS-2 would occur on-orbit using the same lunar scan technique developed to assess the scattering in L8/TIRS.

This article documents the mitigation and assessment process for the TIRS-2 instrument including the discovery of the problem on L8/TIRS, the design changes made to TIRS-2, the preflight measurements of the instrument, the modifications to the optical model, and the final on-orbit assessments of scattering in the instrument.

II. TIRS Stray Light Discovery and Fix

During the Landsat 8 TIRS commissioning in Spring 2013, a radiometric anomaly was observed in Earth imagery from the instrument. Banding, defined as a low-frequency variation across the image, seemed to be pervasive in Earth imagery even in areas expected to be uniform (e.g., open water). The effect was inconsistent from scene to scene and varied as a function of the out-of-field radiance distribution [2]. In addition to the visual banding artifact, the absolute radiometric accuracy of TIRS varied significantly relative to vicarious calibration results based on *in situ* measurements. Calibration errors resulted in image products having an apparent temperature bias of approximately $+2.1$ K and $+4.4$ K for the 10.8 and 12.0 μm bands, respectively, for typical scene temperatures [6]. All data from on-board calibration sources and telemetry, however, indicated that the instrument itself was stable and the anomaly was only observed in Earth imagery.

A possible explanation to both these effects was out-of-field radiance scattering in the optical system and onto the focal plane detectors. Such a stray light effect would allow the detectors to *see* part of the out-of-field scene and add extra signal to the detectors. In this scenario, the magnitude of the extra signal would vary across the detectors and be dependent on the specific view geometry through the optical system and on the content of the out-of-field area.

To confirm this hypothesis, a series of lunar scans were planned to place the Moon just outside of the FOV of the instrument [2]. While aimed at deep space, the detectors should only record background noise. Any signal detected above the background would indicate an unwanted stray light path from the out-of-field Moon through the optical system and onto the focal plane. The exact off-axis angles of the source relative to the TIRS optical axis could be calculated through knowledge of the pointing attitude of the spacecraft and ephemeris data of the Moon. Five lunar scans were performed in which TIRS was aimed in a wide, grid-like pattern around the Moon while recording image data in the transmit-all detector mode to observe the 2-D shape of any potential scatter. (Note that under the usual push-broom mode of imaging, the 2-D structure of the scattering signal would not be imaged by the detector arrays.) After image processing, a noticeable scattering signal was observed when the Moon was approximately 13° from the optical axis, outside the nominal $\pm 7.5°$ FOV of the instrument. A fainter signal was also noticed approximately 22° off-axis. The lunar scans demonstrated that the TIRS instrument suffered from a scattering anomaly that caused banding artifacts and absolute radiometric errors observed in Earth imagery (see [2] for details).

The lunar scan data provided a list of directions and magnitudes for the observed scattering. This dataset only coarsely sampled the out-of-field area given that the Moon is a 0.5° diameter source and that there were approximately 15 scan lines across a $\pm 15°$ field centered on the optical axis (across-track). The dataset was sufficient, however, to provide enough reference data to compare with an optical model. As described in Montanaro *et al.* 2015 [3], the Zemax optical modeling software was used to produce reverse ray trace maps originating from various locations on the detector arrays. The parameters in the model (e.g., surface reflectances) were iterated until the reverse ray trace maps matched the observed lunar data. It was determined that the physical cause of the primary (13°) scattering feature was a stronger than expected reflection from a mechanical bracket in front of the third telescope lens. This path allowed out-of-field radiance to reflect into the telescope on the same side of the instrument. That is, radiance reflected from the left edge of the FOV added signal to the left-side detectors and vice versa for the right-side detectors. The optical model also revealed a weaker reflection from the mechanical bracket behind the second telescope lens that caused the scatter feature observed at 22°. This reflection caused the opposite geometry in which radiance reflected from the left edge of the FOV scattered to the right side of the detectors, and vice versa [3].

As will be discussed later, the information provided by the lunar-based optical model will directly lead to design changes for the TIRS-2 instrument. Although it was impossible to make any physical changes to the TIRS instrument on-orbit, a substantial effort was made to develop an analytic solution to remove the artifacts of stray light in imagery. The optical model was used to generate reverse ray traces of each detector element of the focal plane. These ray traces were effectively maps that provide the direction and weight of the scatter paths from the detector element projected into object space (onto the Earth's surface). Each detector has a different map due to its unique view geometry through the optical system [3]. Ideally, if the exact out-of-field radiance distribution of the particular Earth image was known, then the stray light maps could be used to sample that out-of-field radiance and calculate the amount of signal to be subtracted from that detector element. Simultaneous image data from a sensor with a wider FOV could provide such out-of-field knowledge but obtaining such data over all Earth scenes was not feasible. Alternatively, the stray light maps could be used to sample the TIRS Earth data itself on a scene-by-scene basis to estimate the extra signal to

be subtracted for each detector element. In this case, pixels on the edge of the FOV in the scene are used as a surrogate for the actual out-of-field radiance. This alternative sampling method is currently implemented as the stray light correction algorithm in the USGS Landsat 8 image processing system [7]. The final form of the algorithm only incorporates maps of the 13° sources because incorporating the 22° source maps did not improve the corrected imagery significantly. Extensive analysis has showed that the algorithm reduces the stray light artifacts in both spectral channels to about 1% and vastly improves the visual banding in Earth imagery [7]–[9].

III. TIRS-2 Design and Preflight Characterization

One of the primary changes for the design and integration of the TIRS-2 instrument was to reduce or eliminate the stray light anomalies experienced with TIRS. TIRS-2 was required to be a near-clone of the TIRS design which meant minimal physical changes between the two instruments [1]. Therefore, instead of a complete redesign of the optical system, a slight modification to the existing design was derived from ray tracing analysis of the lunar-verified TIRS optical model to specifically target the scattering angles. Mechanical baffles were installed in front of the third lens in the telescope assembly to reduce the primary scattering at 13° source angles yet keep vignetting effects to a minimum. In addition, analysis from TIRS also indicated a weaker scattering at 22° angles. Initially, these scattering sources were not observed in TIRS on-orbit data but subsequent analysis confirmed a weak signal slightly above the background noise. Another set of unique baffles were added behind the second telescope lens to reduce this 22° scattering feature (see Fig. 1) [5].

Stray light is effectively a component of the overall radiometric uncertainty error budget [10]. The TIRS-2 team determined that a 30x reduction of the signal at 13° and a 3x reduction of the signal at 22° would allow TIRS-2 to meet its radiometric uncertainty requirement with margin. The optical model of the updated telescope design with baffles indicated residual weak scattering sources concentrated around two lobes at 13° on either side of the focal plane along with a diffuse scattering annulus between 20° and 25°. Although the relative magnitude of the stray light model extends over the full field (±30°), the absolute signal ratio of the model had sufficient uncertainty that direct measurements were needed to confirm and refine the optical model.

A comprehensive preflight testing campaign was performed to confirm the impact of the modifications to the TIRS-2 telescope [4]. The instrument was tested in a thermal vacuum (TVAC) chamber to reproduce flight-like conditions with the optical lenses at 190 K and the focal plane below 40 K. The Calibration Ground Support Equipment (CGSE) was placed in the TVAC chamber in front of the TIRS-2 boresight. Among other instrument performance characterization tools, CGSE includes a variable-aperture, variable-temperature blackbody with associated optics to collimate and steer the source radiance through a range of angles relative to the TIRS-2 boresight. Ideally, this CGSE source would be scanned throughout the entire ±30° out-of-field area of the instrument

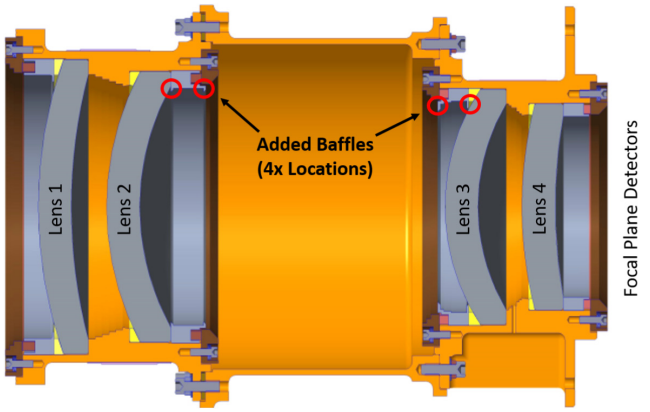

Fig. 1. Cross section of the TIRS-2 telescope assembly indicating the locations of the added baffles to reduce the effect of scattering over the baseline design.

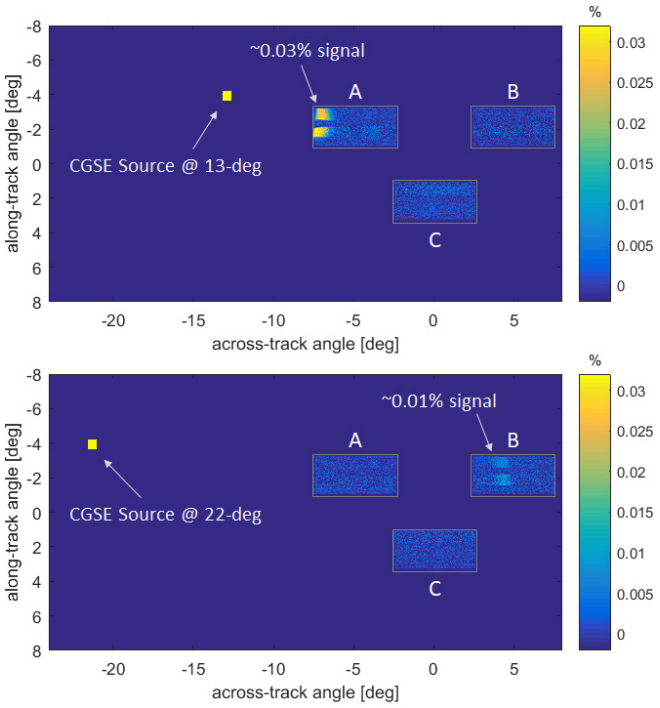

Fig. 2. Processed image data from TVAC measurements of the three TIRS-2 detector arrays (labeled A, B, and C) showing the scattering signal while the CGSE source was positioned at 13° off-axis (top) and positioned at 22° off-axis (bottom). The position of the source relative to the optical boresight is indicated by the yellow square.

to characterize all angles of potential scattered light. However, due to the physical limitations of CGSE and the instrument-to-CGSE geometry, only a limited portion of the TIRS-2 out-of-field area could be scanned between −28° and +18° in the azimuth (across-track) direction and between −8° and +12° in the elevation (along-track) direction [5].

The procedure for measuring scatter involved selecting the 0.7° aperture mask for the CGSE blackbody source and positioning it in a grid between the scan-able field angles. To maximize sensitivity of the measurement, the CGSE blackbody was set to its maximum temperature of 500 K (nominally 240–360 K) and the TIRS-2 detector integration time was set

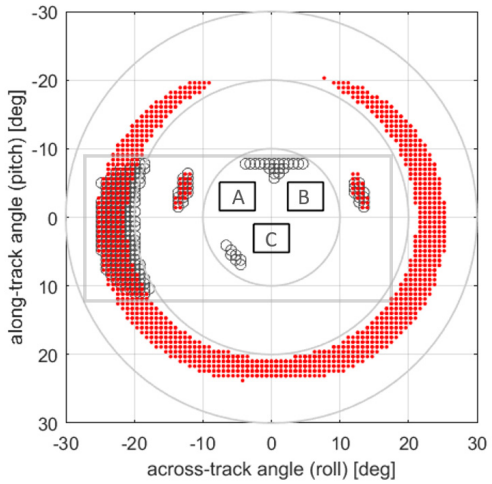

Fig. 3. Map of the out-of-field scattering source locations identified by the optical model (red dots) and by the TVAC measurements (black circles). The rectangular area indicates the angular extent of the TVAC measurements. The three focal plane detector arrays along with concentric circles, indicating 10°, 20°, and 30° boresight angles, are shown as reference.

to its maximum value of 5.5 ms (nominally 2.4 ms). At each source grid location, image data were acquired with the source illuminating TIRS-2 and then with the CGSE shutter closed to serve as a background measurement. Most of the grid locations for the CGSE source were positioned in the out-of-field area; however, when the source was directly illuminating the detectors, a lower integration time allowed for an unsaturated measurement of the direct CGSE signal. All the image data were processed by subtracting the background frames from the source images and then scaling any detectable signals as a fraction of the direct CGSE source signal (after accounting for integration time differences). Therefore, any recorded signals are expressed as a percent of the source radiance for the particular location of the source. Signals above a threshold (determined by trial and error) were flagged as potential scatter and the associated source angles were recorded [5].

The results from the TVAC measurements show that the overall scattering in TIRS-2 was significantly reduced relative to L8/TIRS. As illustrated in Fig. 2, residual scattering from the 13° source angles was approximately 0.03% and scattering from 22° source angles was approximately 0.01%. Scattering at these angles in L8/TIRS was 0.4% and 0.024% for the 13° and 22° angles, respectively, [5]. The total dataset from TVAC measurements was condensed to a list of source angles and the associated magnitude of the scattering on each portion of the detector arrays. A map of the scattering geometry relative to the focal plane detectors is illustrated in Fig. 3 along with the predicted scattering locations from the optical model (red dots) and measured scattering locations (black circles). Although the entire out-of-field area could not be scanned (the scan grid envelope is indicated by the gray rectangle in Fig. 3), the measurements acquired were sufficient to encompass most of the residual scattering sources in the azimuthal direction. The locations (angles) of the measured scattering agree with the predicted scattering angles from the optical model. However, as there was uncertainty into the absolute magnitude of the optical model, the relative magnitudes of the model were combined with the absolute magnitudes derived from TVAC measurements to produce a full-field stray light model of TIRS-2.

The process to scale the optical model magnitude to the TVAC measurements involved comparing areas that overlap between the model and measurements. As illustrated in Fig. 4, TVAC measurements were mostly acquired on the left side and middle of the FOV. The left-side 22° feature, detectable on detector array B, was captured in both the TVAC measurements (Fig. 4, left) and in the model (Fig. 4, middle). Therefore, this area was used to scale the model to the TVAC magnitude by first summing the total signal in this area in the model and summing the total in the TVAC measurements. The ratio of these sums was then applied to the entire model (Fig. 4, right).

The adjusted model was next used to calculate the total predicted signal due to scattering for every detector element across the instrument FOV. The reverse ray traces through the model provided all scattering source angles and their associated magnitudes for each detector. The sum of these scattering sources as a function of detector element yielded an estimate of the total scatter signal expected as a function of FOV angle. This is analogous to the Earth filling the out-of-field area where the scattering signals from all out-of-field angles contribute to a total extra signal across the detector arrays. The predicted total signal for TIRS-2 compared with the total scatter signal from L8/TIRS is shown in Fig. 5. The results essentially provided the amount of extra signal expected in a TIRS image across the width (i.e., FOV) of the image. Whereas the majority of the scatter signal affected the center of the FOV for L8/TIRS, the opposite is true for TIRS-2 in which the edges and not the center of the FOV are affected. The scatter signal of about 1.6% at the extreme ends of the FOV, although greatly reduced from L8/TIRS, still violated the instrument requirement limit of 0.4% total scattering. A waiver to the requirement was submitted after subsequent modeling demonstrated that even with an extreme case of the instrument observing a 260 K in-field source on the Earth surrounded by a 330 K out-of-field source, the resulting absolute radiometric error would be approximately 1.7% (versus a 2% absolute requirement limit for those scene temperatures [10]). In addition, the fact that the TVAC measurements did not encompass the entire out-of-field area left a lingering uncertainty that there could be scattering sources not represented by the optical model. The TIRS-2 instrument project opened an official risk documenting this uncertainty and planned to conduct on-orbit lunar scans similar to L8/TIRS to retire the model uncertainty.

IV. TIRS-2 On-Orbit Characterization

After launch on 27 September 2021, the Landsat 9 observatory and instruments performed a four-month activation and commissioning campaign to power on, test, and calibrate all the components. As part of the commissioning plan for TIRS-2, a series of extended lunar scans were scheduled around the full Moon to provide the final on-orbit assessment

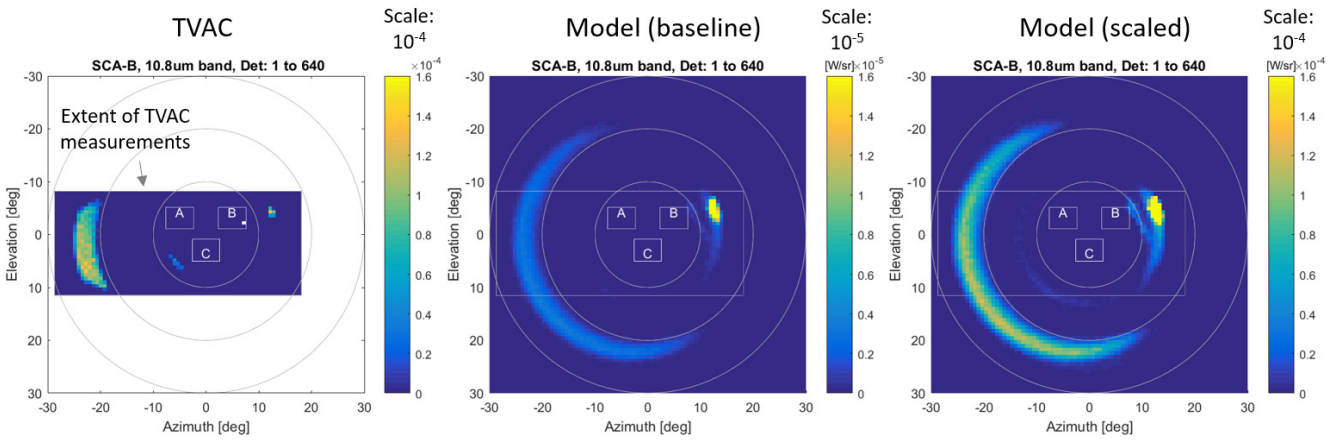

Fig. 4. Left: Illustration of the total scattering locations (as a function of field angle) recorded by detector array B during TIRS-2 TVAC characterization. Blue color indicates no scattering detected for those angles. Middle: the optical model total scattering for detector B encompasses the entire ±30° out-of-field area but magnitudes are only in a relative sense. Right: the TVAC measurements were used to scale the entire optical model to produce a full field model consistent with TVAC measurements.

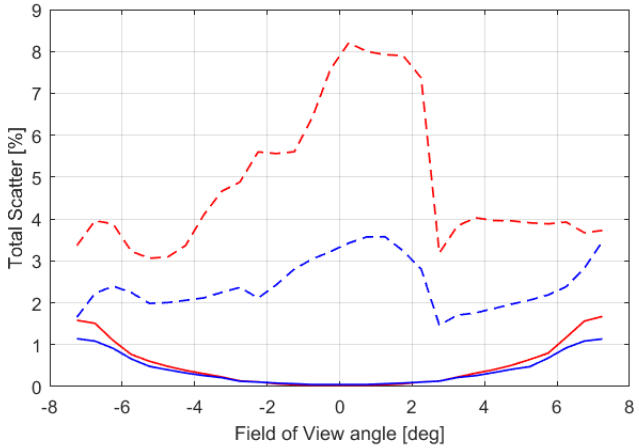

Fig. 5. Total extra signal due to stray light across the FOV for L8/TIRS (dashed lines) and for L9/TIRS-2 (solid lines) for both spectral bands (red for 12.0 μm band and blue for 10.8 μm band). These totals were calculated from the associated optical models.

of scattering in the optical system. The lunar scans for L8/TIRS were needed to confirm the stray light hypothesis and then to feed those measurements into a new optical model. However, the lunar scans for L9/TIRS-2 were used to confirm the existing optical model by taking measurements over a larger out-of-field area that could not be accessed with preflight TVAC measurements. The goal was to demonstrate that the magnitude and locations of the scattering sources were no greater than the prelaunch optical model predicted.

The lunar scans developed for L8/TIRS were used as a template for the L9 scans but were modified to scan a larger portion of the out-of-field area including out to 28° in the across-track direction. A single scan involved the spacecraft's attitude control system (ACS) rotating all the three axes of the L9 observatory to aim the TIRS-2 optical boresight through three vertical (along-track) sweeps with the Moon nearby, but out of, the direct FOV of the detectors. The instrument acquired a continuous stream of images over the approximately 15 minutes the ACS needed to perform its maneuvers. Eight total lunar scans were performed during L9 commissioning spread out over four orbits on two separate days. The number and shape of the scans were planned beforehand to fit in the overall commissioning timeline (i.e., interleaved with other activities) yet provide enough image data early in the mission to assess the TIRS-2 optical model.

The scan images were acquired and processed similar to preflight TVAC measurements. The TIRS-2 detectors operated in the transmit-all mode to acquire a series of frames throughout the lunar scan maneuver. The detector integration time was increased to the maximum value of 5.5 ms to allow for a higher signal-to-noise ratio on any detected scattering. The image data were processed using a frame average with the Moon positioned well outside the optical boresight (greater than 40°) as the background frame to subtract from all other frames. Given that the observatory was in a non-nominal pointing attitude during scans, a correction needed to be applied to account for background drift as a function of time. Around the same time as the extended lunar scans were acquired, a series of direct lunar scans were also performed in which the Moon was directly imaged by TIRS-2 (for calibration purposes). These direct lunar scans were acquired with a lower integration time to permit the Moon, an approximately 400 K source, to be imaged without saturating the detectors. The direct lunar scans allowed the image data from the extended lunar scans to be scaled to an absolute magnitude, after compensating for different integration times. Therefore, all the image data from the extended lunar scans were expressed in terms of fractional direct Moon signal. In the resulting image data, any signals above a threshold were flagged and investigated as potential scattering. For such image frames, the location of the Moon relative to the instrument boresight was calculated using the ACS pointing quaternion telemetry along with Earth and Moon ephemeris data. The complete dataset contained a list of scattering magnitudes for each detector array and the associated lunar location relative to the detectors.

The results confirmed that the scattering in TIRS-2 was greatly reduced from the scattering in TIRS. An example of

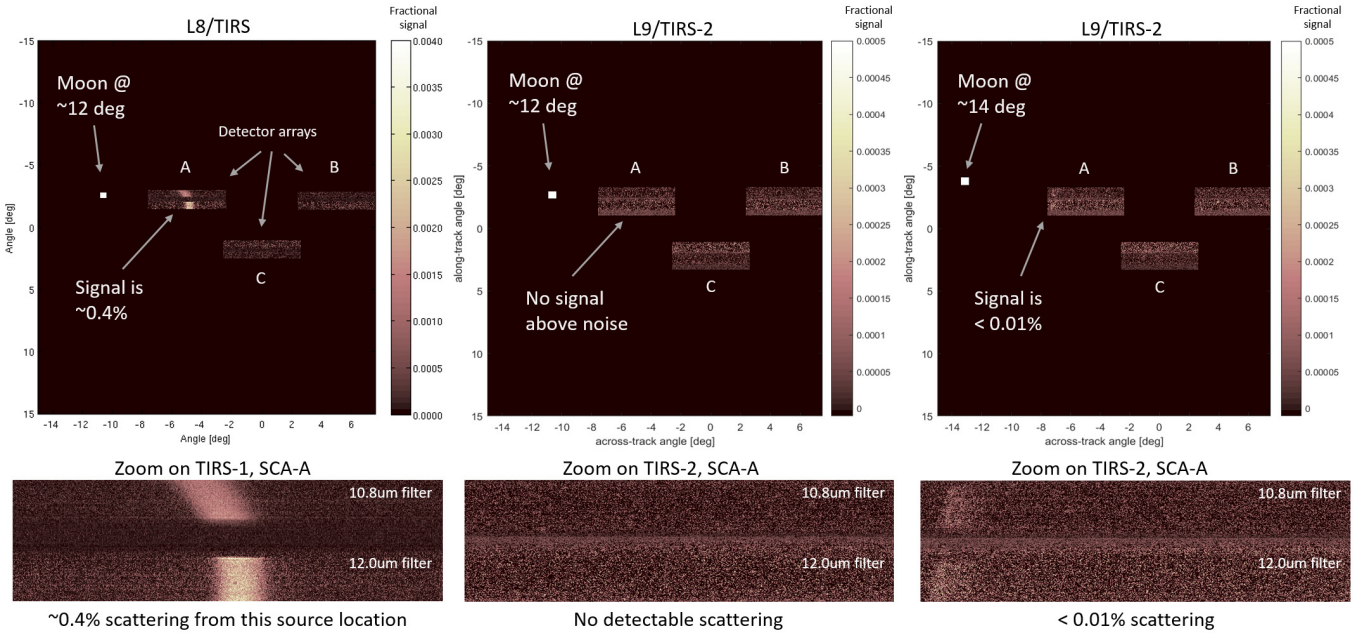

Fig. 6. On-orbit lunar image data from the scattering scans. Left: one L8/TIRS frame with the Moon located approx. 13° off-axis and producing a noticeable scatter signal on detector array A. Middle: the same Moon location does not produce a detectable signal for L9/TIRS-2. Right: the worst case Moon position for TIRS-2 produces a small scattering signal of less than 0.01%. The bottom figures are close-ups of detector array A.

a direct comparison between the observed lunar scattering in L8/TIRS and L9/TIRS-2 is presented in Fig. 6. Recall from L8/TIRS that the primary scattering source was located approximately 13° off-axis, and the added baffles to the TIRS-2 optical system were designed to mostly block these scattering angles. The highest magnitude scattering in TIRS of about 0.4% occurred when the Moon was located in a large 13° off-axis zone (see Fig. 6, left). With the Moon positioned in the same off-axis location, there was no detectable scattering in TIRS-2 (Fig. 6, middle). The worst case scattering in TIRS-2 of below 0.01% was seen when the Moon was located in the smaller 13° lobe predicted by the optical model and observed in TVAC (Fig. 6, right). This figure clearly demonstrates the dramatic reduction of the primary scattering shape and magnitude in the TIRS-2 optical system and shows that the on-orbit scattering magnitude was lower than TVAC measurements (<0.01% for lunar versus 0.03% for TVAC, for this source location). In addition, the 22° scatter signal was observed as approximately 0.007% in the on-orbit data versus 0.01% magnitude in TVAC measurements and 0.024% magnitude in L8/TIRS.

The image analysis was performed over all frames that were flagged as possible scattering. With the goal of confirming the preflight optical model, the flagged scattering locations were overlaid with the optical model and TVAC measurement locations as illustrated in Fig. 7. The Moon locations while TIRS-2 was imaging during the eight lunar scans are indicated by thin red and blue curves, and locations flagged as scattering sources are indicated by the solid circles. The scattering locations predicted by the optical model are drawn as gray dots and TVAC scattering measurements are yellow open circles. For reference, the three rectangular detector arrays are drawn in the center of the FOV and the three concentric rings indicate off-axis angles of 10°, 20°, and 30°. As seen in the figure, the eight lunar scans mostly targeted the right-hand side of the out-of-field and the larger along-track angles which were locations with limited or no TVAC measurements. The resulting lunar scattering locations agreed well with the predicted scattering locations from the optical model (gray dots in the figure). The lunar scattering observed along the approximate 22° arc on the right-hand side of the out-of-field agreed with the optical model and mirrored the observed scattering on the left-hand side as measured in TVAC ground testing. Similarly, the small source lobes around 13° were consistent among the lunar scans, optical model, and TVAC measurements. Overall, the lunar scattering locations agreed with the optical model, and equally important, the lunar scans did not reveal any new scattering locations that were not predicted by the model.

Another conclusion from the lunar scans was that the scattering magnitudes of any single Moon location were less than the magnitudes predicted by the optical model. Recall that the model absolute magnitude was extrapolated based on the limited TVAC measurements that covered about one-quarter of the total out-of-field area. The scaled model was then used to predict the total out-of-field scattering for each detector. The total predicted scattering was about 1.6% at the edge of the FOV and nearly zero in the center of the FOV, which led to the requirement waiver and official instrument risk. The lunar scans provided actual scattering measurements over a large portion of the out-of-field and concretely demonstrated that the optical model scattering locations were accurate and the predicted magnitudes were higher than the actual observed scattering. Therefore, the predicted magnitudes of the model are now seen as a worst case magnitude. The lunar scans

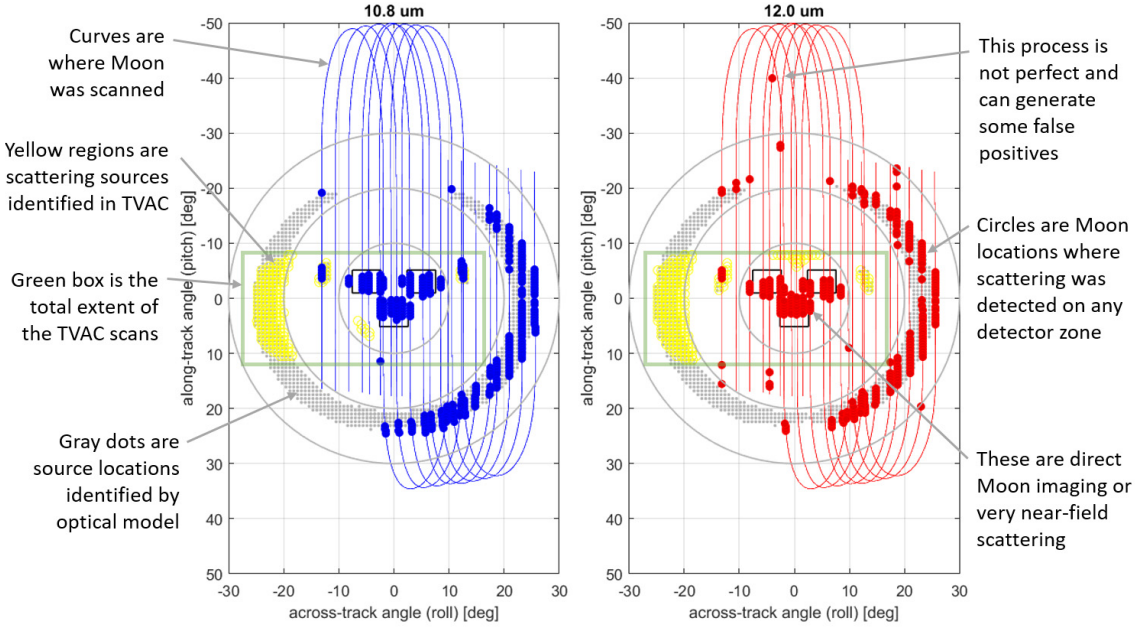

Fig. 7. Total scattering maps for TIRS-2 for the 10.8 μm band (left) and 12.0 μm band (right). Similar to the data in Fig. 3, the predicted scattering locations from the optical model are indicated by gray dots, while yellow data points are sources identified by TVAC measurements. Blue and red curves illustrate the locations of the Moon as image data were collected during scans. Large blue and red dots are Moon locations where scatter was observed on the detectors.

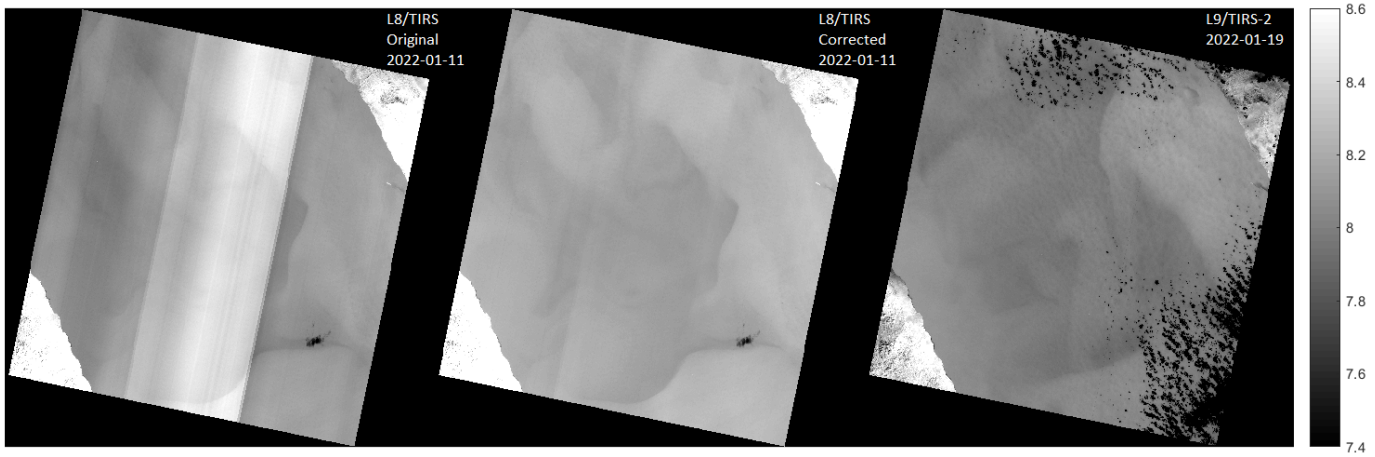

Fig. 8. Red sea (WRS2 path 173/row 42) Landsat product images acquired by the 12.0 μm band on TIRS instruments and processed through the USGS ground system with a contrast scale in units of radiance (W/m^2/sr/μm). Left: image acquired by L8/TIRS on 2022-01-11 with processing originally available to users (with a 0.51 W/m^2/sr/μm bias removed). Middle: the same image from L8/TIRS but with full stray light correction processing applied [7]. Most of the stray light artifacts have been removed with some residual banding. Right: the L9/TIRS-2 image of the same location (but different day, 2022-01-19) showing no observable stray light artifacts (note there are some clouds in the image).

clearly showed that the primary source at 13° was reduced by approximately 40 times over the scattering in L8/TIRS. The secondary source at 22° was reduced by 3 times over the scattering in L8/TIRS. Recall that the added baffles to the TIRS-2 optical system were specifically designed to reduce 13° and 22° scatter magnitudes to targets of 30x and 3x, respectively.

As a final note on the scans, if the lunar data had shown that scattering was much higher than the optical model predicted, then the existing stray light correction process implemented in the Landsat ground processing system for L8/TIRS could have been activated to remove predicted artifacts from TIRS-2 image data [7]. The required steps would involve planning and executing a complete series of lunar scans to cover the remaining out-of-field area with sufficient density to feed back to the optical model. The updated model would then be used to develop reverse ray traces for each individual detector. The ray traces would be fed into the current stray light correction algorithm and the algorithm coefficients rederived for TIRS-2 image data. Fortunately, as the final results of the TIRS-2 on-orbit scans were completed, the National Aeronautics and Space Administration (NASA) and USGS agreed that this course of action along with further lunar scans were not needed and the official risk was retired.

The ultimate verification of stray light mitigation on TIRS-2 is the quality of Earth imagery. Stray light artifacts added up to 8% extra radiance in 12.0 μm band images from L8/TIRS. The

effect varied scene to scene and depended on the distribution of the out-of-field radiance. Imagery of the Red Sea region in the Middle East was a particularly prominent example of the stray light artifacts as the relatively cooler water in the scene contrasted with the warmer desert out-of-field. Ideally, the water should appear uniform across the image but the stray light problem added a non-uniformity that varied as the out-of-field geometry changed from north to south (see Fig. 8, left). The implemented stray light correction algorithm removed the majority of the artifacts and resulted in a nearly uniform image (Fig. 8, middle). The same scene location acquired by L9/TIRS-2 (on a different day, with some clouds) is uniform across the entire image and devoid of stray light artifacts (Fig. 8, right).

V. Summary and Conclusion

The stray light problem inherent to the Landsat 8 TIRS optical system was solved for the Landsat 9 TIRS-2 instrument. A comprehensive campaign to identify, measure, and model the scattering effect in the TIRS instrument while on-orbit led to a detailed understanding of the root cause of the problem. That knowledge was applied to the TIRS-2 instrument design to add strategically placed baffles to the optical system to cut off the identified scattering sources at 13° and 22° off-axis. Through a major preflight characterization operation, the design changes were tested over a limited set of off-axis angles in flight-like conditions in a TVAC chamber and results indicated at least an order of magnitude reduction of scattering. The TVAC measurements confirmed the residual scattering locations predicted by the optical model and were then used to extrapolate and scale the optical model to the entire out-of-field area. Although preflight data confirmed the vast reduction of scattering artifacts, uncertainty still existed about the extent and magnitude of the residual scattering sources and TIRS-2 launched with a known risk of stray light uncertainty. Once on-orbit, a final characterization of the residual stray light was performed by conducting similar lunar scans pioneered by L8/TIRS. The lunar dataset finally confirmed that the primary and secondary scattering sources (at 13° and 22°) have been reduced by 40 times and by 3 times, respectively, over the original TIRS design. Earth imagery acquired by TIRS-2 has not shown any stray light artifacts.

Acknowledgment

The TIRS-2 Integration & Test team at the National Aeronautics and Space Administration/Goddard Space Flight Center (NASA/GSFC) facilitated the TVAC test that allowed for scattering measurements. The Landsat 9 Flight Operations, Flight Dynamics, and Mission Planning teams planned and executed the on-orbit lunar scans. U.S. Geological Survey/Earth Resources Observation and Science Center (USGS/EROS) helped process the TIRS Earth imagery.

References

[1] J. H. Hair *et al.*, "Landsat 9 thermal infrared sensor 2 architecture and design," in *Proc. IEEE Int. Geosci. Remote Sens. Symp. (IGARSS)*, Jul. 2018, pp. 8841–8844.

[2] M. Montanaro, A. Gerace, A. Lunsford, and D. Reuter, "Stray light artifacts in imagery from the Landsat 8 thermal infrared sensor," *Remote Sens.*, vol. 6, no. 11, pp. 10435–10456, 2014. [Online]. Available: https://www.mdpi.com/2072-4292/6/11/10435

[3] M. Montanaro, A. Gerace, and S. Rohrbach, "Toward an operational stray light correction for the Landsat 8 thermal infrared sensor," *Appl. Opt.*, vol. 54, pp. 3963–3978, May 2015. [Online]. Available: http://opg.optica.org/ao/abstract.cfm?URI=ao-54-13-3963

[4] J. McCorkel *et al.*, "Landsat 9 thermal infrared sensor 2 characterization plan overview," in *Proc. IEEE Int. Geosci. Remote Sens. Symp. (IGARSS)*, Jul. 2018, pp. 8845–8848.

[5] M. Montanaro *et al.*, "Landsat 9 thermal infrared sensor 2 preliminary stray light assessment," in *Proc. IEEE Int. Geosci. Remote Sens. Symp. (IGARSS)*, Jul. 2018, pp. 8853–8856.

[6] J. A. Barsi, J. R. Schott, S. J. Hook, N. G. Raqueno, B. L. Markham, and R. G. Radocinski, "Landsat-8 thermal infrared sensor (TIRS) vicarious radiometric calibration," *Remote Sens.*, vol. 6, no. 11, pp. 11607–11626, 2014. [Online]. Available: https://www.mdpi.com/2072-4292/6/11/11607

[7] A. Gerace and M. Montanaro, "Derivation and validation of the stray light correction algorithm for the thermal infrared sensor onboard Landsat 8," *Remote Sens. Environ.*, vol. 191, pp. 246–257, Mar. 2017. [Online]. Available: https://www.sciencedirect.com/science/article/pii/S0034425717300421

[8] A. Gerace, M. Montanaro, and R. Connal, "Leveraging intercalibration techniques to support stray-light removal from Landsat 8 thermal infrared sensor data," *Proc. SPIE*, vol. 12, no. 1, pp. 1–13, 2017, doi: 10.1117/1.JRS.12.012007.

[9] M. Montanaro and A. Gerace, "Performance of the proposed stray light correction algorithm for the thermal infrared sensor (TIRS) onboard Landsat 8," *Proc. SPIE*, vol. 9972, pp. 120–126, Sep. 2016, doi: 10.1117/12.2238554.

[10] A. Pearlman *et al.*, "Prelaunch radiometric calibration and uncertainty analysis of Landsat thermal infrared sensor 2," *IEEE Trans. Geosci. Remote Sens.*, vol. 59, no. 4, pp. 2715–2726, Apr. 2021.

Matthew Montanaro received the B.S. degree in physics and the Ph.D. degree in imaging science from the Rochester Institute of Technology (RIT), Rochester, NY, USA, in 2005 and 2009, respectively.

He has been involved in the calibration of imaging sensors through NASA Goddard Space Flight Center since 2009. He has supported the prelaunch and on-orbit calibration of the Landsat 8/Thermal Infrared Sensor (TIRS), the Landsat 9/TIRS-2, and the Lucy/Ralph instruments and will continue calibration work for the upcoming Landsat Next project.

Joel McCorkel, photograph and biography not available at the time of publication.

June Tveekrem, photograph and biography not available at the time of publication.

John Stauder, photograph and biography not available at the time of publication.

Eric Mentzell, photograph and biography not available at the time of publication.

Allen Lunsford, photograph and biography not available at the time of publication.

Jason Hair, photograph and biography not available at the time of publication.

Dennis Reuter, photograph and biography not available at the time of publication.